Electronic Transport in Natively Oxidized Silicon Nanowires

Mohammad Koleini,[†,*] Lucio Colombi Ciacchi,[†,‡] and Maria Victoria Fernández-Serra[§]

[†]Hybrid Materials Interfaces Group, Faculty of Production Engineering and Bremen Center for Computational Materials Science, University of Bremen, 28359 Bremen, Germany, [‡]Fraunhofer Institute for Manufacturing Technology and Applied Materials Research IFAM, 28359 Bremen, Germany, and [§]Department of Physics and Astronomy and New York Center for Computational Science, Stony Brook University, Stony Brook, New York 11794-3800, United States

ABSTRACT Silicon nanowires are widely used as active functional elements in advanced electronic devices, most notably in biological sensors. While surface oxidation of the wires occurs upon exposure to a wet environment, theoretical studies are often limited to ideally crystalline, H-terminated wire models. We present an accurate computational study of the electronic and transport properties of natively oxidized, ultrathin silicon nanowires including dopant elements. Comparisons with perfectly ordered and distorted H-terminated structures reveal an unexpected interplay of effects that oxidation-induced structural distortions and electronegative Si/SiO_x interfaces have on the conductance of B- or P-doped nanowires.

KEYWORDS: silicon nanowires · surface oxidation · quantum transport · molecular electronics · nanowire doping

Silicon nanowires (SiNWs) are among the most promising fundamental building blocks for the fabrication of nanostructured functional devices.[1] The synthesis of Si and other semiconductor nanowires can follow either a bottom-up route, notably by means of chemical vapor deposition techniques,[2] or a top-down route fully compatible with well-established SOI and CMOS technologies.[3] This makes SiNWs ideally suited as conducting elements in field effect transistors (FET)[4] or highly sensitive sensors for the label-free detection of biological molecules.[3,5] In either cases, the wires' functionality results from their electronic conduction properties. These in turn depend on the wire morphology and the type and concentration of dopants,[6−8] as investigated in numerous experimental studies of the SiNWs' atomistic[9,10] and electronic[6,11,12] structures.

Depending on the synthesis route and the application environment, the exposed surfaces of SiNWs are either hydrogen-terminated[13] or passivated by an ultrathin oxide layer.[14] Ultrathin nanowires have been grown successfully in different groups, with a diameter as low as 13 Å in one of the thinnest (embedded) SiNWs[13] fabricated up to now. This small size opens the possibility to study the entire system by means of detailed theoretical methods. However, most atomistic simulations to date have focused on the properties of undoped and non-oxidized wires,[15−21] mostly because of the lack of realistic models for Si/SiO_x core−shell wire structures. In particular, theoretical studies dealing with the transport properties of pure and doped SiNWs have been performed for model structures where the dangling bonds at the wire surfaces are saturated with hydrogen atoms.[22−28]

In this paper, we study the transport properties of B- and P-doped ultrathin SiNWs covered with a hydroxylated native oxide layer, building upon previous simulation studies of the oxidation,[29] water reaction,[30] and dopant segregation[31] of Si surface slabs. The importance of considering the effect of surface oxidation on the wire's properties is motivated by numerous applications in which SiNWs are either exposed to a wet environment, as in the case of SiNW biosensors,[3,5] or in contact with a SiO_2 insulation layer, such as in FinFETs.[32]

RESULTS AND DISCUSSION

While many previous transport studies on doped SiNWs focused on the [110] direction, a complete atomistic model for an oxidized and hydrated surface is available for the [100] direction only,[29,30] which is the starting point to construct our oxidized [100] wire structure. Namely, we start from a 2×2×2 64-atom primitive silicon unit cell periodically repeated along the z direction (the wire axis) and terminated in the $\pm x$ and $\pm y$ directions by the oxidized and hydroxylated Si(001) surface model generated in ref 30 for a 2 × 2 surface unit cell. To relax the defects introduced in this way at the wire's edges, we manually remove obvious steric clashes, include terminal OH groups, and perform classical MD simulations at 300 K with the force field developed in ref 33 for Si/SiO_x interfaces, applying a Nosé−Hoover

* Address correspondence to koleini.m@gmail.com.

Received for review December 7, 2010 and accepted March 4, 2011.

Published online March 04, 2011
10.1021/nn103363y

© 2011 American Chemical Society

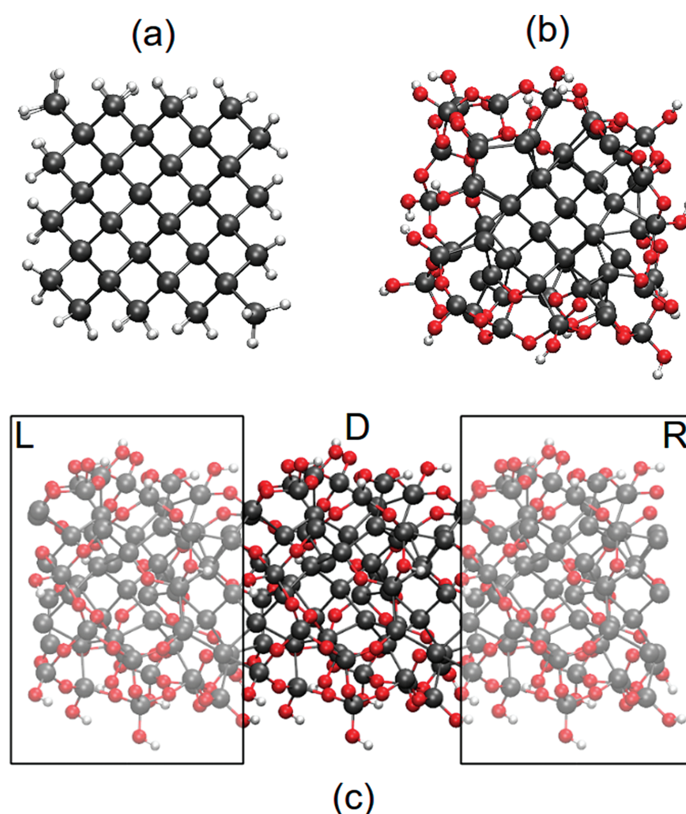

Figure 1. [100]-Grown wires. (a) Cross-section of hydrogen-passivated pristine wire. (b) Cross-section of the oxidized wire. (c) Lateral view of the oxidized wire. The left and right contacts used in the transport calculations are depicted as watermarked unit cells.

thermostat and an integration time step of 1 fs. These operations are repeated until we obtain a core−shell structure free from under-coordination or over-coordination defects of all Si atoms. Finally, we perform an accurate 0.5 ps *ab initio* MD annealing and geometry relaxation at the full DFT level, until all force components on all atoms are below 0.05 eV/Å.

The finally obtained structure contains 58 O atoms, which either are in a bridge configuration between two Si atoms or belong to terminal hydroxyl groups, and 63 Si atoms (one Si atom having been removed during the construction of the oxide shell). The oxidized wire presents a well-defined silicon core, although with evident distortions from the ideal lattice structure, as can be observed in Figure 1b. An analogous pristine H-terminated wire is constructed simply by saturating the dangling bonds of the 64-atom Si cell with 60 hydrogen atoms (Figure 1a). Neglecting the effect of surface strains due to the different surface terminations (which results in less than 1% difference in the optimized axial lattice parameters), we use a repeating unit cell along the wire direction of 10.91 Å in both cases, while the wire diameters are about 13 and 16 Å for the H-terminated and oxidized case, respectively. Transport properties are computed for periodically repeated lead/device/lead structures consisting of three identical unit cells (Figure 1c). To our best knowledge, this is the first transport study of such a complex nanowire with full-scale DFT calculations, whereas previous studies have provided useful insights of simplified model systems, mostly using more approximated approaches such as tight-binding.[34,35]

We begin our study with a comparison of the band structures computed for the pristine and oxidized wires. With respect to the H-terminated wire, the oxidized wire band gap is reduced from 2.6 to 1.2 eV, and the bands become less dispersive (Figure 2a,c). This effect can partially be ascribed to the presence of an oxide shell with a larger dielectric constant than Si, leading to a reduced quantum confinement, as shown by Niquet *et al.*[36] Moreover, it has been shown in ref 37, for the case of ideally crystalline SiNWs terminated with −OH groups, that a combination of reduced quantum confinement and hybridization of Si valence band with the termination groups leads to a reduction of the band gap. A further origin of quantum confinement reduction in our oxidized wire is the structural distortions of the crystalline lattice around and in the silicon core, which will obviously reduce the dispersion of the Si states along the wire axis. To highlight the contribution of structural disorder, we have computed the band structure of a H-terminated wire with a distorted structure, obtained after MD annealing of the pristine wire constraining the atoms in the core to the same

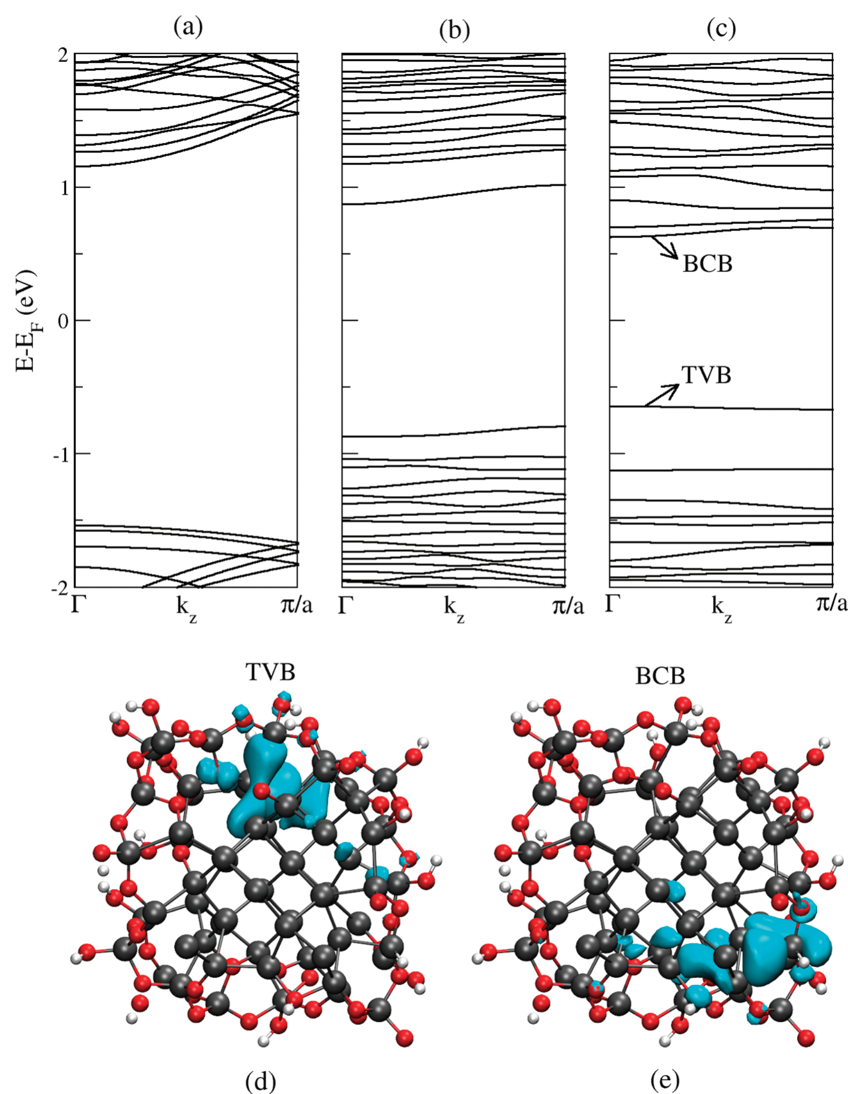

Figure 2. Band structures of (a) pristine, (b) prisitine distorted, and (c) oxidized SiNWs. (d) Top of valence band (TVB) and (e) bottom of conduction band (BCB) states in the oxidized SiNW pertaining to the marked bands shown in (c).

positions as in the oxidized wire (see Figure S1 in the Supporting Information). Notably, applying these distortions changes the band gap from 2.6 to 1.7 eV (Figure 2), proving that structural disorder significantly contributes to reducing the band gap and the band dispersion.

In Figure 2d,e, we show the electronic density plot associated with states at the top of the valence band and the bottom of the conduction band of the oxidized wire. These states are localized at the interface between the Si core and the oxide shell of the wire, with high densities located in Si−O bonds. This suggests that the presence of a Si/SiO_x interface may intrinsically affect the wire's transport properties, which are studied below.

Differently from the case of SiNWs exposing reconstructed {100} surfaces,[38] our wires are free from Si dangling bonds and thus have no electronically conducting states at the Fermi level. To analyze the wire transmission in a realistic device, we thus introduce p-type (boron) or n-type (phosphorus) dopant atoms, in line with previous studies.[22,23,26] Before computing the transport properties, we investigate the possible surface or interface segregation of dopants by means of total-energy calculations.

In the case of the pristine wire, due to the symmetry of the structure, there are two chemically different sites for substitutional B and P impurities, namely, at the surface and in the core of the wire. The energy difference, $\Delta E = E_{surface} - E_{core}$, is 0.03 and 0.22 eV for B and P dopants, respectively, showing that no surface segregation of the dopants is expected. In the case of the oxidized wire, the Si atoms can be distinguished depending on the number of neighbor oxygen atoms. The total energy of wires with the dopant in all possible oxidized sites and in relevant core positions are plotted in Figure 3. Consistently with the results obtained for the case of oxidized Si(001) surface slabs,[31] both B and P dopants are more stable

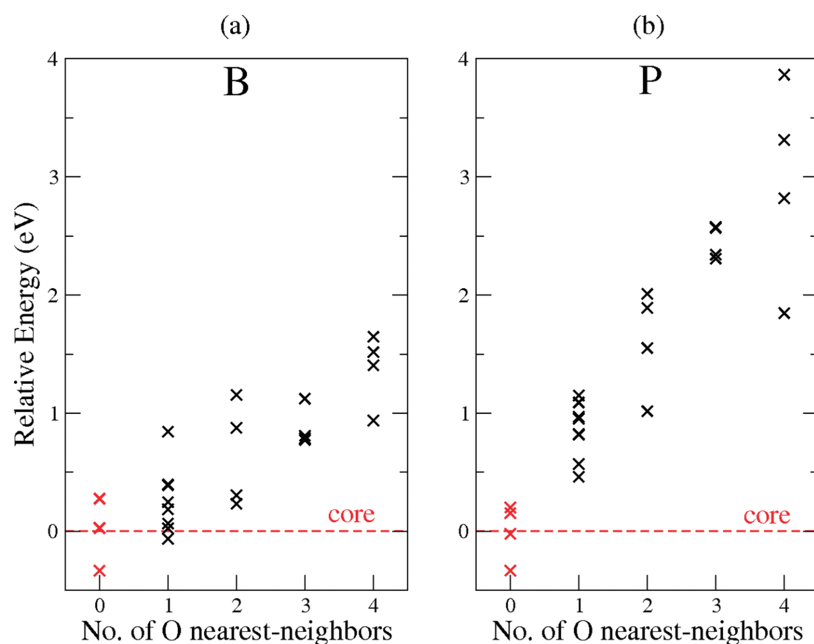

Figure 3. (a) Boron and (b) phosphorus dopant energetics.

in the silicon core region, with the total energy increasing roughly linearly with the number of O neighbors.

The band structure and partial density of states (PDOS) of the pristine and oxidized wires doped with B and P are shown in the Supporting Information (Figure S2). In all cases, there is a band crossing the Fermi level, making the wire potentially conducting. For B-doping and P-doping, the band gap amounts to 2.51 and 2.56 eV for the pristine wires and 1.63 and 1.44 eV for the oxidized wires, respectively. The density of states projected on the dopant atom and its four nearest neighbors shows that states localized at and around the dopant site are present at the Fermi level and will thus influence the wires' electronic transport.

Our transport calculations are based on the non-equilibrium Green's function method.[39] We consider here a regime of low bias and linear response and calculate the transmission spectra from

$$T_e(\varepsilon) = \mathrm{Tr}[\Gamma_L \mathbf{G}^a \Gamma_R \mathbf{G}^r](\varepsilon) \qquad (1)$$

where the advanced (retarded) Green's function, $\mathbf{G}^{a(r)}$, is calculated from the Hamiltonian and self-energies of the device region, and $\Gamma_\alpha(\varepsilon) = -2\mathrm{Im}[\sum_\alpha(\varepsilon)]$, with $\alpha = L,R$. As mentioned, the system used in the transport calculations consists of three unit cells repeated along the z direction, serving as the left electrode, the device region, and the right electrode (see Figure 1). To ensure that the length of the device region is long enough to prevent the overlap of orbitals of the electrodes with each other, a transmission spectrum calculation with two unit cells in the device region has been performed, which showed no appreciable difference from the case of a single unit cell.

The transmission spectra calculated for the doped pristine, pristine distorted, and oxidized wires are shown in Figure 4, while the corresponding spectra for the undoped case are reported in the Supporting Information (Figure S3). The spectra of the doped pristine wire show noninteger drops of transmission at about −1.0 or +0.6 eV for the case of B and P, marked with arrows in Figure 4a,d. Similar signatures were observed by Fernández-Serra *et al.*[23] in doped [110]-oriented SiNWs and attributed to backscattering effect. In our case, however, they might originate also from the less dispersed band structure along the [100] direction. The gap visible in the spectrum of the B-doped pristine wire below the Fermi level is clearly due to the strong energy localization of the B-induced electronic state above the valence band maximum (see Figure S2a). Introducing structural disorder in the pristine wire leads to decreased transmission probability (Figure 4b,e), effectively suppressing the incoming wave functions at all energy levels. In the oxidized wire, the transmission probability is reduced even more, and the spectra exhibit a dense series of discrete transmission channels with energy widths of the order of hundreds of millielectronvolts, which reflects the flattening of the electronic bands in the near-gap region. In some cases, these narrow channels overlap with each other, causing broader and higher transmission features. In both the B-doped and the P-doped cases, there is exactly one channel conducting at the Fermi level.

The electronic conductance G at the Fermi level at room temperature can be computed using the Landauer formula:

$$G = G_0 \int_{-\infty}^{\infty} \mathrm{d}\varepsilon T_e(\varepsilon) \left(-\frac{\partial f(\varepsilon, \mu)}{\partial \varepsilon} \right) \qquad (2)$$

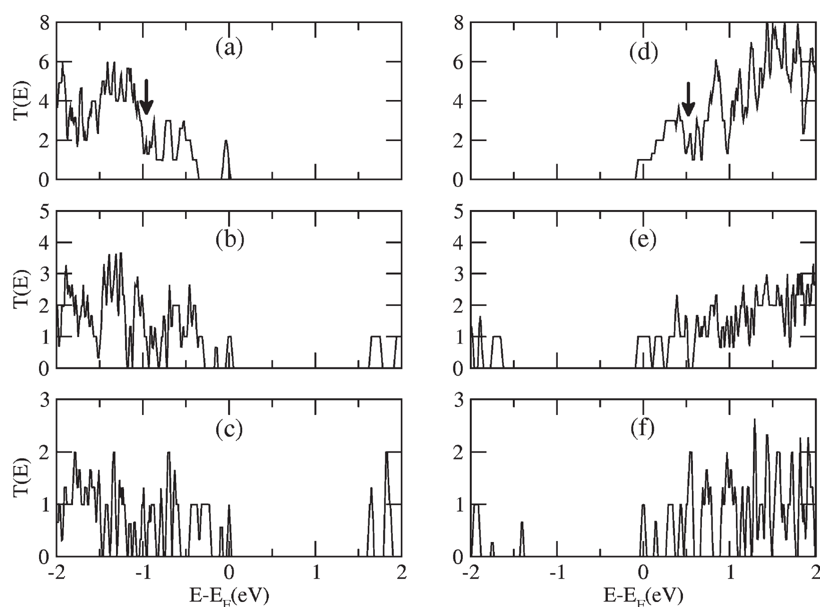

Figure 4. Transmission spectra of B-doped (a) pristine, (b) pristine distorted, (c) oxidized and P-doped (d) pristine, (e) pristine distorted, (f) oxidized wires.

TABLE 1. Electronic Conductance of Doped SiNWs at the Fermi Level at Room Temperature, in Units of G_0, along with the Standard Deviation (σ) Obtained from Eight Independent Calculations with the Dopant in Different Core Sites

dopant	pristine (σ)	pristine distorted (σ)	oxidized (σ)
B	0.74 (0.00)	0.43 (0.14)	0.43 (0.09)
P	0.95 (0.00)	0.89 (0.06)	0.41 (0.11)

where $G_0 = 2e^2/h$ is the quantum of conductance and $f(\varepsilon,\mu) = 1/(\exp[(\varepsilon - \mu)/k_BT] + 1)$ is the Fermi-Dirac distribution function at the chemical potential μ (the Fermi level in our calculations). On the basis of this formula, we have calculated the conductances of the doped wires. The results are summarized in Table 1. Because of symmetry, in the case of pristine wires, the values of G are insensitive to the specific dopant site. In the case of distorted and oxidized wires, the reported values are the averages of eight different calculations with the dopant in different sites inside the Si core.

Our calculations reveal that the conductance of pristine wires is slightly higher for P-doping than for B-doping. This is understandable from the higher effective mass of holes along the [100] direction,[25,40] which results from a smaller dispersion and thus in a smaller mobility than in the case of electrons.[23] Introducing structural distortions leads to a decrease of the conductance which is much larger for B-doped than for P-doped wires. To rationalize this observation, we look at the spatially resolved scattering states of the transmission eigenchannels at the Fermi level,[41] as depicted in Figure 5. These are roughly correspondent to the electronic states at the valence band maximum (for B) or conduction band minimum (for P), as shown in Figure S4 of the Supporting Information. For doped pristine wires, we observe that in the case of P-doping the eigenchannel is localized in close proximity of the dopant site, whereas it is evidently delocalized in the case of B-doping (Figure 5a,c). This is consistent with the fact that the strength of the hydrogenoid-type potential for the electron induced by P is much larger than the correspondent potential for the hole induced by B, as shown by Fernández-Serra *et al.*[23] We can thus expect the conductance of small radius B-doped wires to be strongly affected by structural distortions spread across the whole wire core. Instead, in similar wires, the more localized eigenchannel of the P-doped wire should be less perturbed by the structural disorder, as indeed reflected by the calculated values of G. However, the oxidation of the wire's surface changes this behavior. The shell provides electronegative sites at the Si/SiO_x interface, which attract the additional electron introduced by the P dopant, as confirmed by visual analysis of the state at the bottom of the conduction band for P-doped oxidized wires (Figure S4d). This results in a delocalization of the transmission eigenchannels over a large portion of the wire (including the interface region) also in the case of P-doping (Figure 5d) and to an associated strong decrease of the conductance at the Fermi level to values now very similar for either dopant element (Table 1).

We stress that these results are in part a consequence of the small size of our crystalline SiNW core. A different behavior can be expected for larger crystalline cores, since the dopant-induced resonant backscattering is stronger for P-doped than for B-doped wires due to the stronger nature of the impurity potential.[23] In this case, we expect that the resonant

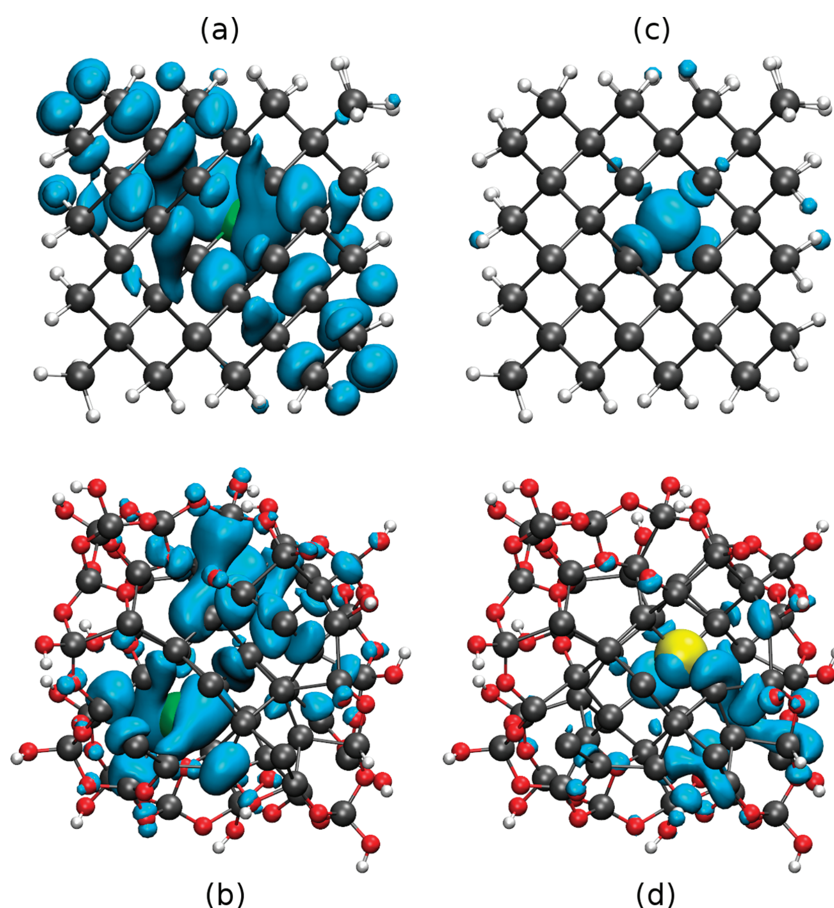

Figure 5. First transmission eigenchannels of (a) pristine wire, B-doped; (b) oxidized wire, B-doped; (c) pristine wire, P-doped; (d) oxidized wire, P-doped. Green and yellow spheres depict boron and phosphorus, respectively; to show them clearly, their sizes have been increased to half of their van der Waals radii. Two pristine wires (a,c) and two oxidized wires (b,d) each have the same isosurface cutoff.

backscattering induced by P impurities could be reduced upon oxidation, thanks to the competing attractive potential for the electron induced by the oxide shell. The same oxide shell will act as a stronger confining potential for the holes provided by B impurities. Which of the two options, namely, doping with B or P, will result in larger conductance will depend on the level of segregation of the dopant atoms toward the core. If impurities are more stable in the core region, as shown here for small radius wires, we expect P-doping (n-type) to be more efficient. In addition, we note that the strength of the impurity-induced scattering potentials does depend on the size of the unit cell along the wire's axis.[42,43] Therefore, future detailed thermodynamical and kinetic studies of the distribution of impurities in larger oxidized wires will be necessary to achieve more definitive conclusions, allowing for the inclusion of realistically long-ranged impurity potentials.

While our study is limited to the [100] wire growth direction, we expect our conclusion about the effects of an oxide shell and of a disordered Si lattice in the near-oxide region to hold qualitatively also for other directions. However, the inherent anisotropy of the Si band structure is at the origin of different effective masses and thus different mobilities for holes and electrons along different directions, especially for small wires subjected to quantum confinement effects.[25,44] Persson *et al.* have estimated effective masses along [100] to be $m^* = 0.30m_0$ and $m^* = 0.97m_0$ for electrons and holes in pristine SiNWs, respectively, while the corresponding values along [110] are $m^* = 0.14m_0$ and $m^* = 0.18m_0$.[25] Therefore, at least for the case of B-doping, transport in [100]-oriented SiNW devices may be hindered by the low carrier mobility. Interestingly, the presence of a native oxide layer results in a considerable flattening of both the valence and the conduction bands (see Figure 2), indicating that the associated reduced mobility of the carriers could severely limit the conductivity of thin wire devices. The dependence of these effects on the crystallographic direction is an issue that shall be investigated in further studies, in which oxidized wire models grown along the [110] direction should be constructed and their transport properties evaluated and compared with the results presented here.

Finally, it needs to be mentioned that, before a direct comparison to experimental observables can be made,

further studies shall be devoted to contemplate issues such as possible shortcomings of the DFT-GGA method, the effect of a bias electric field on the transmission, or the occurrence of other scattering sources and Anderson localization in real devices.

CONCLUSIONS

In summary, we have studied the electronic and transport properties of ultrathin, natively oxidized and doped SiNWs grown along the [100] direction. We have shown that the surface oxidation of the wires induces structural distortions of the wire core and changes its quantum confinement,[36] decreasing the band gap and providing less dispersive states. Dopants have been found to be stable in the wire's core, in the absence of coordination defects at the Si/SiO_x interface. The conductance of the oxidized wires is decreased with respect to the case of ideally crystalline, H-terminated wires, due to the combined effect of the structural distortions induced by the oxidation process and of the presence of electronegative sites at the Si/SiO_x interface. The overall conductance decrease is very similar for B and P dopants, despite the fact that the transmission of P-doped wires is less influenced by structural disorder in the absence of an oxide shell. The use of either p- or n-type doping is thus not expected to have a marked effect on the performance of oxidized nanowire devices (at least for small diameter sizes), so that the choice of the more suitable kind of dopant can be taken on the basis of other fabrication considerations.

COMPUTATIONAL METHODS

In our calculations, we use density functional theory (DFT) within a generalized gradient approximation to the exchange and correlation functional[45] as implemented in the SIESTA code.[46] The nuclei and core electrons are replaced by norm-conserving pseudopotentials,[47] and the Kohn−Sham electronic states are expressed as linear combinations of strictly localized numerical atomic orbitals. We use a double-ζ polarized basis set with an energy shift of 0.02 Ry and a grid cutoff of 300 Ry. A 16 k-point grid is used to sample the reciprocal space along the wire axis. In dopant energetics calculations, in order to avoid basis set superposition errors (BSSE) intrinsic in methods based on finite basis sets, the dopants' energetics calculations have been performed by plane-wave method implemented in ref 48 using ultrasoft pseudopotentials with a 32 Ry (320 Ry) cutoff for the wave functions (charge density).

Acknowledgment. This work has been partially supported by the Land Bremen and the Deutsche Forschungsgemeinschaft (Emmy Noether Grant CI 144/2-1). The work at Stony Brook University was supported by DOE Award Number DE-FG02-09ER16052. Computer time has been allocated at the University of Bremen, at the HLRN, Hannover, and at the ZIH, Dresden. M.K. and L.C.C. are members of the ISIS Sensorial Materials Scientific Centre, Bremen.

Supporting Information Available: Figures S1, S2, S3, and S4 mentioned in the text are included. This material is available free of charge *via* the Internet at http://pubs.acs.org.

REFERENCES AND NOTES

1. Rurali, R. Colloquium: Structural, Electronic, and Transport Properties of Silicon Nanowires. *Rev. Mod. Phys.* **2010,** *82*, 427–449.
2. Lu, W.; Lieber, C. Nanoelectronics from the Bottom Up. *Nat. Mater.* **2007,** *6*, 841–850.
3. Stern, E.; Klemic, J.; Routenberg, D.; Wyrembak, P.; Turner-Evans, D.; Hamilton, A.; LaVan, D.; Fahmy, T.; Reed, M. Label-Free Immunodetection with CMOS-Compatible Semiconducting Nanowires. *Nature* **2007,** *445*, 519–522.
4. Cui, Y.; Zhong, Z.; Wang, D.; Wang, W.; Lieber, C. High Performance Silicon Nanowire Field Effect Transistors. *Nano Lett.* **2003,** *3*, 149–152.
5. Stern, E.; Vacic, A.; Li, C.; Ishikawa, F.; Zhou, C.; Reed, M.; Fahmy, T. A Nanoelectronic Enzyme-Linked Immunosorbent Assay for Detection of Proteins in Physiological Solutions. *Small* **2010,** *6*, 232–238.
6. Cui, Y.; Duan, X.; Hu, J.; Lieber, C. Doping and Electrical Transport in Silicon Nanowires. *J. Phys. Chem. B* **2000,** *104*, 5213–5216.
7. Ma, D.; Lee, C.; Lee, S. Scanning Tunneling Microscopic Study of Boron-Doped Silicon Nanowires. *Appl. Phys. Lett.* **2001,** *79*, 2468.
8. Lew, K.; Pan, L.; Bogart, T.; Dilts, S.; Dickey, E.; Redwing, J.; Wang, Y.; Cabassi, M.; Mayer, T.; Novak, S. Structural and Electrical Properties of Trimethylboron-Doped Silicon Nanowires. *Appl. Phys. Lett.* **2004,** *85*, 3101.
9. Wu, Y.; Cui, Y.; Huynh, L.; Barrelet, C.; Bell, D.; Lieber, C. Controlled Growth and Structures of Molecular-Scale Silicon Nanowires. *Nano Lett.* **2004,** *4*, 433–436.
10. Menon, M.; Srivastava, D.; Ponomareva, I.; Chernozatonskii, L. Nanomechanics of Silicon Nanowires. *Phys. Rev. B* **2004,** *70*, 125313.
11. Cui, Y.; Lieber, C. Functional Nanoscale Electronic Devices Assembled Using Silicon Nanowire Building Blocks. *Science* **2001,** *291*, 851.
12. Yu, J.; Chung, S.; Heath, J. Silicon Nanowires: Preparation, Device Fabrication, and Transport Properties. *J. Phys. Chem. B* **2000,** *104*, 11864–11870.
13. Ma, D.; Lee, C.; Au, F.; Tong, S.; Lee, S. Small-Diameter Silicon Nanowire Surfaces. *Science* **2003,** *299*, 1874.
14. Schmidt, V.; Wittemann, J.; Gosele, U. Growth, Thermodynamics, and Electrical Properties of Silicon Nanowires. *Chem. Rev.* **2010,** *110*, 361–388.
15. Ismail-Beigi, S.; Arias, T. Edge-Driven Transition in the Surface Structure of Nanoscale Silicon. *Phys. Rev. B* **1998,** *57*, 11923–11926.
16. Zhao, Y.; Yakobson, B. What is the Ground-State Structure of the Thinnest Si Nanowires? *Phys. Rev. Lett.* **2003,** *91*, 35501.
17. Singh, A.; Kumar, V.; Kawazoe, Y. Pristine Semiconducting [110] Silicon Nanowires. *Nano Lett.* **2005,** *5*, 2302–2305.
18. Kagimura, R.; Nunes, R.; Chacham, H. Structures of Si and Ge Nanowires in the Subnanometer Range. *Phys. Rev. Lett.* **2005,** *95*, 115502.
19. Ponomareva, I.; Menon, M.; Srivastava, D.; Andriotis, A. Structure, Stability, and Quantum Conductivity of Small Diameter Silicon Nanowires. *Phys. Rev. Lett.* **2005,** *95*, 265502.
20. Zheng, Y.; Rivas, C.; Lake, R.; Alam, K.; Boykin, T.; Klimeck, G. Electronic Properties of Silicon Nanowires. *IEEE Trans. Electron Devices* **2005,** *52*, 1097–1103.
21. Ng, M.; Zhou, L.; Yang, S.; Sim, L.; Tan, V.; Wu, P. Theoretical Investigation of Silicon Nanowires: Methodology, Geometry, Surface Modification, and Electrical Conductivity Using a Multiscale Approach. *Phys. Rev. B* **2007,** *76*, 155435.

22. Fernández-Serra, M.; Adessi, C.; Blase, X. Surface Segregation and Backscattering in Doped Silicon Nanowires. *Phys. Rev. Lett.* **2006,** *96*, 166805.
23. Fernández-Serra, M.; Adessi, C.; Blase, X. Conductance, Surface Traps, and Passivation in Doped Silicon Nanowires. *Nano Lett.* **2006,** *6*, 2674–2678.
24. Svizhenko, A.; Leu, P.; Cho, K. Effect of Growth Orientation and Surface Roughness on Electron Transport in Silicon Nanowires. *Phys. Rev. B* **2007,** *75*, 125417.
25. Persson, M.; Lherbier, A.; Niquet, Y.; Triozon, F.; Roche, S. Orientational Dependence of Charge Transport in Disordered Silicon Nanowires. *Nano Lett.* **2008,** *8*, 4146–4150.
26. Markussen, T.; Rurali, R.; Jauho, A.; Brandbyge, M. Scaling Theory Put into Practice: First-Principles Modeling of Transport in Doped Silicon Nanowires. *Phys. Rev. Lett.* **2007,** *99*, 76803.
27. Markussen, T.; Jauho, A.-P.; Brandbyge, M. Electron and Phonon Transport in Silicon Nanowires: Atomistic Approach to Thermoelectric Properties. *Phys. Rev. B* **2009,** *79*, 035415.
28. Markussen, T.; Rurali, R.; Cartoixà, X.; Jauho, A.-P.; Brandbyge, M. Scattering Cross Section of Metal Catalyst Atoms in Silicon Nanowires. *Phys. Rev. B* **2010,** *81*, 125307.
29. Ciacchi, L.; Payne, M. First-Principles Molecular-Dynamics Study of Native Oxide Growth on Si(001). *Phys. Rev. Lett.* **2005,** *95*, 196101.
30. Colombi Ciacchi, L.; Cole, D.; Payne, M.; Gumbsch, P. Stress-Driven Oxidation Chemistry of Wet Silicon Surfaces. *J. Phys. Chem. C* **2008,** *112*, 12077–12080.
31. Cole, D.; Payne, M.; Colombi Ciacchi, L. Stress Development and Impurity Segregation during Oxidation of the Si(100) Surface. *Surf. Sci.* **2007,** *601*, 4888–4898.
32. Hisamoto, D.; Lee, W.; Kedzierski, J.; Takeuchi, H.; Asano, K.; Kuo, C.; Anderson, E.; King, T.; Bokor, J.; Hu, C. FinFET—A Self-Aligned Double-Gate MOSFET Scalable to 20 nm. *IEEE Trans. Electron Devices* **2002,** *47*, 2320–2325.
33. Cole, D.; Payne, M.; Csányi, G.; Spearing, S.; Ciacchi, L. Development of a Classical Force Field for the Oxidized Si Surface: Application to Hydrophilic Wafer Bonding. *J. Chem. Phys.* **2007,** *127*, 204704.
34. Pecchia, A.; Salamandra, L.; Latessa, L.; Aradi, B.; Frauenheim, T.; Di Carlo, A. Atomistic Modeling of Gate-All-Around Si-Nanowire Field-Effect Transistors. *IEEE Trans. Electron Devices* **2007,** *54*, 3159–3167.
35. Fagas, G.; Greer, J. Ballistic Conductance in Oxidized Si Nanowires. *Nano Lett.* **2009,** *9*, 1856–1860.
36. Niquet, Y.; Lherbier, A.; Quang, N.; Fernandez-Serra, M.; Blase, X.; Delerue, C. Electronic Structure of Semiconductor Nanowires. *Phys. Rev. B* **2006,** *73*, 165319.
37. Nolan, M.; O'Callaghan, S.; Fagas, G.; Greer, J.; Frauenheim, T. Silicon Nanowire Band Gap Modification. *Nano Lett.* **2007,** *7*, 34–38.
38. Rurali, R.; Lorente, N. Metallic and Semimetallic Silicon ⟨100⟩ Nanowires. *Phys. Rev. Lett.* **2005,** *94*, 26805.
39. Brandbyge, M.; Mozos, J.; Ordejón, P.; Taylor, J.; Stokbro, K. Density-Functional Method for Nonequilibrium Electron Transport. *Phys. Rev. B* **2002,** *65*, 165401.
40. Sanders, G.; Stanton, C.; Chang, Y. Theory of Transport in Silicon Quantum Wires. *Phys. Rev. B* **1993,** *48*, 11067–11076.
41. Paulsson, M.; Brandbyge, M. Transmission Eigenchannels from Nonequilibrium Green's Functions. *Phys. Rev. B* **2007,** *76*, 115117.
42. Diarra, M.; Niquet, Y.; Delerue, C.; Allan, G. Ionization Energy of Donor and Acceptor Impurities in Semiconductor Nanowires: Importance of Dielectric Confinement. *Phys. Rev. B* **2007,** *75*, 45301.
43. Rurali, R.; Markussen, T.; Suñé, J.; Brandbyge, M.; Jauho, A. Modeling Transport in Ultrathin Si Nanowires: Charged *versus* Neutral Impurities. *Nano Lett.* **2008,** *8*, 2825–2828.
44. Niquet, Y. M.; Genovese, L.; Delerue, C.; Deutsch, T. *Ab Initio* Calculation of the Binding Energy of Impurities in Semiconductors: Application to Si Nanowires. *Phys. Rev. B* **2010,** *81*, 161301.
45. Perdew, J.; Burke, K.; Ernzerhof, M. Generalized Gradient Approximation Made Simple. *Phys. Rev. Lett.* **1996,** *77*, 3865–3868.
46. Soler, J.; Artacho, E.; Gale, J.; Garcia, A.; Junquera, J.; Ordejon, P.; Sanchez-Portal, D. The SIESTA Method for *Ab Initio* Order-N Materials Simulation. *J. Phys.: Condens. Matter* **2002,** *14*, 2745.
47. Troullier, N.; Martins, J. Efficient Pseudopotentials for Plane-Wave Calculations. *Phys. Rev. B* **1991,** *43*, 1993–2006.
48. Giannozzi, P.; Baroni, S.; Bonini, N.; Calandra, M.; Car, R.; Cavazzoni, C.; Ceresoli, D.; Chiarotti, G. L.; Cococcioni, M.; Dabo, I.; *et al.* QUANTUM ESPRESSO: A Modular and Open-Source Software Project for Quantum Simulations of Materials. *J. Phys.: Condens. Matter* **2009,** *21*, 395502.